Friction during earthquakes: 25 years of experimental studies

Friction during earthquakes: 25 years of experimental studies

G Di Toro[1,2], S Aretusini[2], C Cornelio[2], S Nielsen[3], E Spagnuolo[2], A Núñez-Cascajero[4], A Tapetado[4], C Vázquez[4]

[1]Dipartimento di Geoscienze, Università degli Studi di Padova, Via G. Gradenigo 1, Padua, Italy
[2]Istituto Nazionale di Geofisica e Vulcanologia, Via di Vigna Murata 605, Rome, Italy
[3]Department of Earth Sciences, Durham University, South Road, Science Site, Durham, Great Britain
[4]Departamento Tecnología Electrónica, Universidad Carlos III de Madrid, Av. Universidad 30, Leganés, Spain

Abstract. Dynamic fault strength τ (rock friction in the broad sense) and its evolution with seismic slip and slip rate are among the most relevant parameters in earthquake mechanics. Given the large slip rate (1 m s^{-1} on average), displacement (up to tens of meters), effective stress (tens of MPa), typical of seismic faulting at depth, thermo-mechanical effects become outstanding: dynamic fault strength is severely affected by fluid and rock phase changes, extreme grain size reduction, and the production of amorphous and unstable materials in the slipping zone. Here, first we will summarize the most relevant findings about dynamic fault strength during seismic slip mainly obtained thanks to the exploitation of dedicated experimental machines (i.e., rotary shear apparatus). However, the interpretation of this experimental dataset remains debated because of technical limitations which impede us to measure fundamental parameters such as temperature, strain rate, pore fluid pressure and grain size in the slipping zone. Without a sound estimate of these physical parameters, any constitutive law proposed to describe the evolution of dynamic fault strength during simulated seismic slip remains speculative. Then, we will discuss the results of some recent experiments which exploit new technical approaches to overcome the main limitations of the previous studies. The experimental approach, together with field studies of the geometry and architecture of exhumed faults and modelling, remains our most powerful tool to investigate seismic-related deformation mechanisms in both natural and human-induced earthquakes.

1. State of the art

Dynamic fault strength τ (rock friction in the broad sense) and its evolution with seismic slip and slip rate control the nucleation, propagation and arrest of seismic ruptures [1]. Geological evidence shows that seismic slip is localized in < 2 cm slip zones during earthquakes [2-4]. Given the low thermal conductivity of rocks, the large slip rate (up to 10 m/s), displacement (up to tens of meters), effective stress (tens of MPa), typical of seismic faulting at depth, thermo-mechanical effects become outstanding [5]:

$$\Delta T = \frac{\tau V_{\text{slip}} \sqrt{t}}{c_p \rho \sqrt{\alpha_{\text{th}} \pi}} \quad (1)$$

with ΔT the temperature increase (K), τ shear stress (MPa), V_{slip} slip rate (m s^{-1}), t time (s), c_p specific heat (J K^{-1} kg^{-1}), ρ rock density (kg m^{-3}) and α_{th} thermal diffusivity (m^2 s^{-1}). From Eq. 1, by introducing typical values for crystalline silicate built rocks (c_p = 1000 J K^{-1} kg^{-1}, ρ = 2700 kg m^{-3} and $\alpha_{\text{th}} = 10^{-6}$ m^2 s^{-1}) and expected shear stresses (50 MPa at slip initiation) and seismic slip rates (1 m s^{-1}) on a fault patch at 6 km depth, in the slipping zone we would expect a bulk temperature increase of about 1000 K after only 1 cm of slip. As a consequence, dynamic fault strength is severely affected by fluid and rock phase changes, extreme grain size reduction, and the production of amorphous and unstable materials in the slipping zone (Fig. 1).

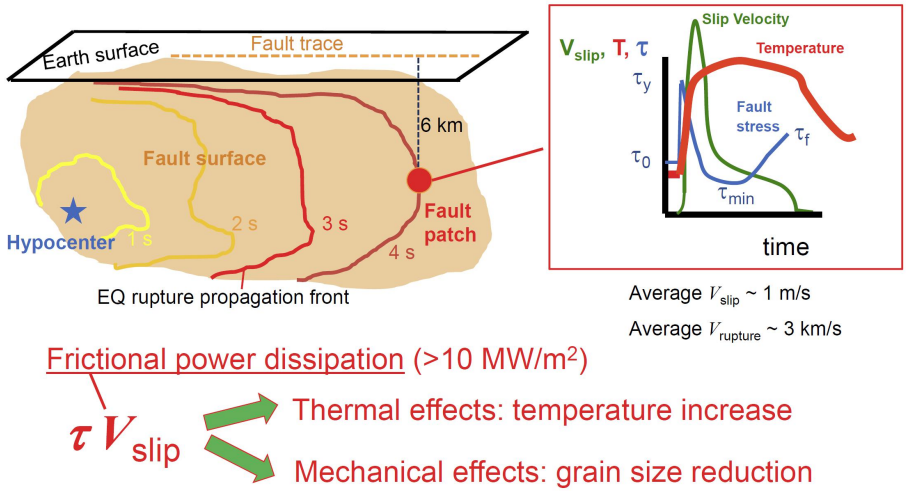

Figure 1. During earthquakes, the passage of the rupture front at ~3 km/s along a fault (light brown in color) patch results in large stress perturbations. During faulting, the shear stress first increases from initial state τ_0 to fault yielding τ_y and then decreases to a minimum value τ_{min} and eventually increases to a final τ_f (blue in color curve). At the same time, just behind the propagating rupture front, fault slip is abruptly accelerated to tens or hundreds m s^{-1} for few ms, though the average fault slip rate V_{slip} on the fault patch over the entire slip event is about 1 m s^{-1} (green curve). The combination of large shear stress and slip rates results in large frictional power dissipation per unit area in the fault slipping zone (tens to hundreds of MW m^{-2} at few km depth in the Earth's crust). Such large frictional dissipation is converted into heat (Eq. 1), which triggers abrupt temperature increase (red curve), and mechanical work which results in grain size reduction and amorphization of the fault rock materials.

Moreover, the presence of fluids (H_2O, CO_2, etc.) in the fault core materials may contribute to dynamic weakening (e.g., fluid thermal pressurization, elasto-hydrodynamic lubrication) and possibly buffer the temperature increase in the slipping zone [5-6].

In the first rupture models proposed in the Sixties of XX century, it was proposed that fault strength during earthquakes decreases inversely with slip rate V_{slip} (enhanced velocity-weakening model [7]:

$$\tau \sim 1/ V_{slip} \quad (2).$$

Given the lack of determination of dynamic fault strength through seismological methods, elucidating constraints may arise from experimental studies. However, the experimental evidence for the strong dependence of fault friction with slip rate has been lacking for decades. Preliminary experimental studies of friction in rocks at seismic slip rates were performed in the Thirties [8] and Eighties [9] of the last century. But it has been only with the installation of dedicated experimental machines ("high-velocity" rotary shear friction machines, [10-13]) that the extreme deformation conditions achieved during earthquakes were approached in the laboratory and systematically investigated. In 1997, Tsutsumi and Shimamoto [14] reported the first experimental data of dynamic fault strength in cohesive rocks at seismic slip rates: this study opened a new era in experimental rock deformation. Several fault dynamic weakening mechanisms first proposed theoretically (i.e., frictional melting lubrication, flash heating & weakening and, more recently, fluid thermo-mechanical pressurization and elasto-hydrodynamic lubrication), were eventually reproduced in the laboratory [e.g., 6,15]. These experiments allowed us also to explore and propose new dynamic fault weakening mechanisms, including silica-gel lubrication [16], grain-size- and temperature-dependent crystal-

plastic weakening [17-19], etc.; other will be probably discovered in the future. Nevertheless, the $\tau \sim 1/ V_{slip}$ relation ["enhanced dynamic weakening", ref. 20] was systematically observed, independently of the rock composition and presence of fluids (Fig. 2).

Nowadays, theoretical thermo-mechanical models, calibrated by experimental measures and microstructural observations, enable us to construct constitutive equations for dynamic fault strength which begin to find application into numerical modeling of earthquakes ruptures for both natural and human-induced seismicity [21].

2. Discussion and conclusions

Despite these recent experimental advancements, the activation of several of the proposed dynamic fault weakening mechanisms and their occurrence in natural faults are debated. In fact, technical challenges of the current experimental approach such as poor estimate of both temperature and pore fluid pressure, or the lack of *in-situ* observations during rock sliding which impede to determine the strain rate and grain size in the slipping zone, limit our understanding of seismic-related deformation mechanisms. Moreover, high-resolution microstructural and microanalytical studies are conducted on *post-mortem* specimens (i.e., slip zone recovered after the experiments).

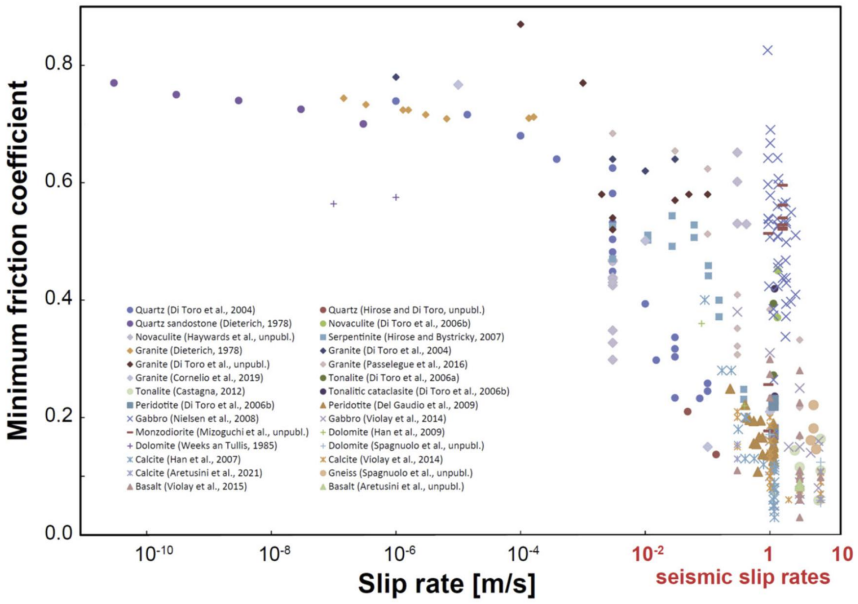

Fig. 2. Enhanced dynamic fault weakening in cohesive rocks (~450 experiments). According to experimental evidence, the minimum dynamic rock friction coefficient (or minimum dynamic fault strength if multiplied by the effective normal stress) in fault rocks independently of their mineralogical composition and specific deformation mechanism, decreases from 0.8-0.7 to 0.02 approaching seismic slip deformation conditions (slip rates of ca. 1 m s^{-1}, normal effective stress of tens of MPa). The scatter of the friction coefficient data observed at seismic slip rates (red fonts) is related to the applied normal stress: for a given rock composition and slip rate, the minimum friction coefficient achieves the lowest values at the highest imposed normal stresses (normal stresses are not reported in the figure) [Figure modified from 20 by adding experiments performed in the period 2012-2021].

Because of the relatively large temperatures achieved in the slipping zone, *post-mortem* microstructures may be affected by annealing and sintering, which overprint and possibly obliterate the microstructures formed and active during simulated seismic slip. For instance, if we consider the

constitutive equation that may describe dynamic fault weakening by crystal plastic and grain-size- and temperature-dependent processes [18-19]:

$$\frac{d\varepsilon}{dt} \sim e^{-\frac{Q}{RT}} \tau^n d^m \quad (3)$$

with $d\varepsilon/dt$ strain rate (s^{-1}), Q "activation energy term" (J mol^{-1} K^{-1}), R gas constant (J mol^{-1}), n stress exponent ($1 \leq n \leq 7$), d grain size with m the grain size exponent ($1 \leq m \leq 3$), critical parameters such as the thickness of the active slipping zone (which would allow us to estimate the strain rate), the temperature in the slipping zone and the grain size of the sheared materials are almost a guess. As a consequence, the application of this kind of constitutive equations, obtained also from experiments performed under very different loading conditions and experimental configurations (gas- and solid-confinement machines, e.g. Paterson rigs and Griggs apparatus) remains questionable. Moreover, in rotary shear configuration, the confinement of gouges and pore fluids is a serious technical issue. The spurious friction of the confining medium (usually Teflon) and the lack of reproducible fluid pressure measurements in the slipping zone renders the interpretation of the mechanical data difficult. Here we will briefly introduce recent technical improvements that allowed us to measure during simulated seismic slip the temperature evolution and, in the case of experiments performed in the presence of fluids, the transient pore fluid pressure in the slipping zone [15,22].

Rock sliding and dynamic frictional strength are related to the interaction of microscale contacts (< 0.1 mm in diameter) called asperities. At slip initiation, the temperature increases in microseconds at the asperity scale. Usually, temperatures are measured by means of thermocouples, which may detect temperature near (< 1 mm) the fault surface. However, thermocouples have a large inertia (~ 0.1 s) compared to the timescale of the earthquake processes (10^{-6}-10^{-5} s) and poor spatial resolution (> 1 mm) compared to the asperity size. Moreover, thermocouples can be cut during sliding and cannot be inserted directly on the slipping zone. Alternatively, Infra-Red (IR) cameras are used, but they have a poor spatial resolution to resolve spatially the asperity contacts and they record the temperature outside of the slipping zone. As a consequence, temperatures in the slipping zone are estimated by means of numerical models calibrated on temperature measurements determined outside of the slipping zone. However, temperature modeling requires strong assumptions (e.g., partitioning between mechanical and thermal energy sinks, changes in thermal conductivity of the rock assemblage, temperature buffering due to phase transitions and mineral breakdown reactions).

Recently, the installation optical fibers on rotary shear configuration allowed us to overcome most of these technical problems. In particular, optical fibers can be inserted directly in the slipping zone, have a very high spatial resolution (< 30 μm) and acquire temperature measurements up to 1 kHz (ideally up to 1 MHz) during simulated seismic slip (Fig. 3, [22]). One of the most intriguing results was that the measured temperatures were hundreds of degrees °C higher than those estimated from modeling. Given the Arrhenius-type dependence of dynamic fault strength with temperature (Eq. 3), the achievement of such high temperatures has profound impact on the activation of different dynamic weakening mechanisms and their transition during seismic slip.

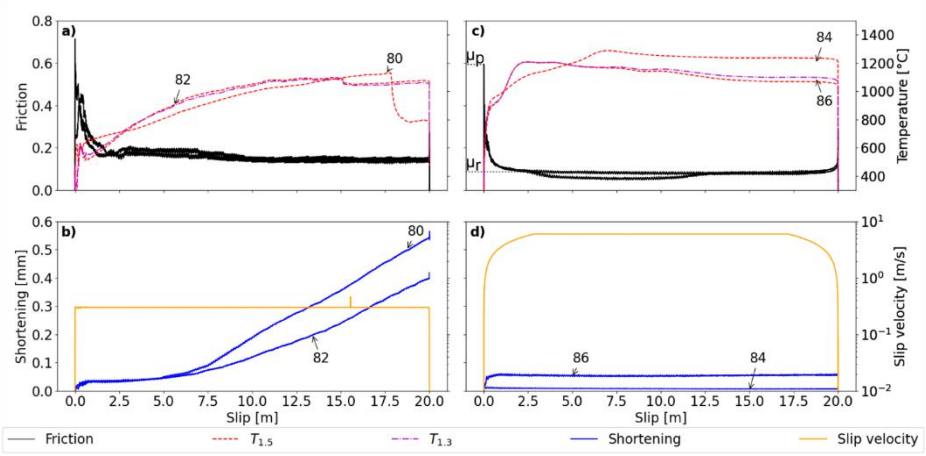

Fig. 3. Temperature increase measured with optical fibers in experiments performed on solid Carrara marble cylinders at a normal stress of 20 MPa. The Carrara marble was sheared at a target slip rate of 0.3 m s^{-1} (Figs. a and b) and 3 m s^{-1} (Figs. c and d) [Figure from 22].

A second technical improvement allowed us to measure short-duration transient pore fluid pressures during simulated seismic slip. Based on theoretical arguments, thermal pressurization of fluids trapped in slipping zones is the most fashioned dynamic weakening mechanism for earthquakes and landslides [e.g., 5,23]. However, detecting these transients is extremely challenging because fluids and gouges must be sealed and confined, respectively, to avoid extrusion under simulated crustal earthquakes. Sample confinement results in spurious friction. The application of a new experimental configuration where fluids and gouges were jacketed with an ultra-low friction lubricated PVC shrink tube and then inserted into a water filled and pressurized fluid vessel allowed us to confine the sample assemblage. Fluids were then injected and pressurized inside the slip zone with a syringe pump and the pore fluid pressure monitored with a pressure transducer. One of the most intriguing results was that, because of the negligible temperature increase measured in the experiments, rather than thermal pressurization due to fluid expansion, was the fluid pressurization due to mechanical compaction that resulted in large dynamic fault weakening in these experiments (Fig. 4). As a consequence, fluid-saturated clay-rich sediments, occurring at shallow depth in subduction zones, can promote earthquake rupture propagation and slip because of their low permeability and tendency to pressurize when sheared at seismic slip velocities.

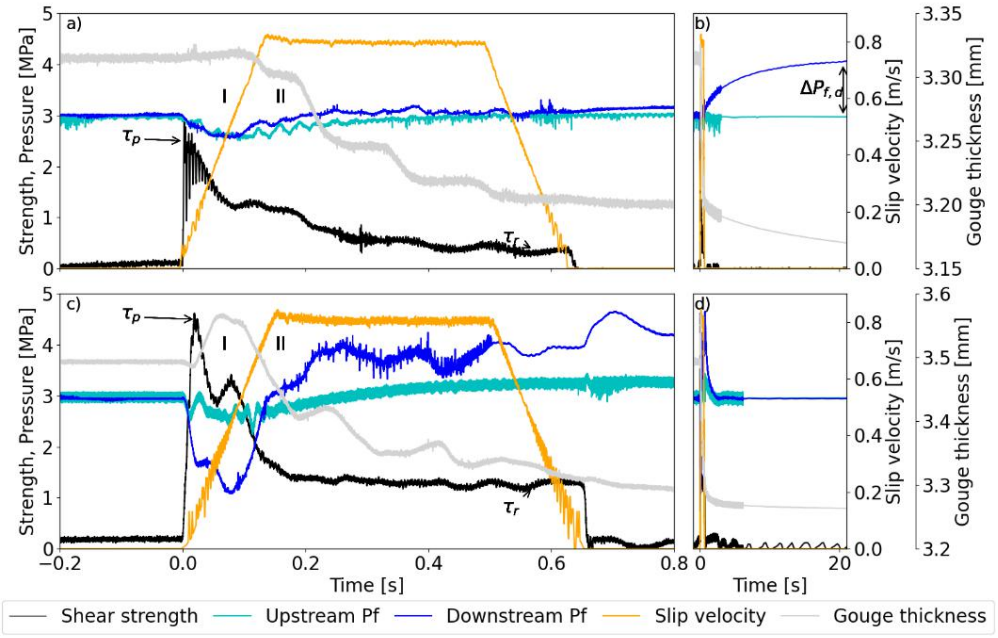

Figure 4. Fluid pressure evolution in clay-rich gouges retrieved from the deep oceanic drilling of the tsunamigenic Pāpaku thrust from the Hikurangi subduction zone off-shore New Zealand (experiment s1737, Figs. a-b) and in calcite Carrara marble gouge (experiment s1823, Figs. c-d). Slip velocity, thickness, shear strength, and pore fluid pressure are presented versus time. Note in b the pressure increase (blue curve) due to fluid mechanical pressurization. This transient is detected *after* the short-living seismic slip pulse (orange curve) because of the low permeability of the Pāpaku thrust gouges. Instead, in the case of the higher permeability calcite gouges (c-d), the pore fluid transient is detected during the slip pulse. In both gouges, dilatancy of the slipping zone (grey curve) at slip initiation resulted in a drop in pore fluid pressure and in an increase in dynamic fault strength (black curve). This dilatancy hardening effect may result in rupture arrest under particular loading condition, though its understanding requires further experimental and theoretical investigations [Figure from 15].

These first experimental results obtained with new experimental configurations may contribute to unravel the dynamic weakening mechanisms activated during seismic slip, and strengthen their respective constitutive laws. These new experimental configurations may also allow us to investigate better the role of effective normal stress and of the loading conditions that lead to the transition between dynamic weakening mechanisms (e.g., initial flash heating and weakening to bulk frictional melting lubrication). However, are the *in-situ* observations of the slipping zone during simulated seismic slip that will contribute also enormously to our understanding of earthquakes physics. In this case, one of the most promising experimental technological improvements, coupled with the exploitation of artificial intelligence and machine learning techniques, is the installation of X-ray transparent vessels in synchrotron radiation facilities [24]. High-resolution *in-situ* dynamic X-ray imaging using X-ray microtomography under the synchrotron beam will probably allow us to “see”, in the near future, what happens in the slipping zone during a simulated earthquake under quite realistic deformation conditions.

3. References

[1] Scholz C H 2019 *The mechanics of earthquakes and faulting*. 3rd edn. (Cambridge, USA: Cambridge University Press).

[2] Chester F M, Chester J S 1998 *Tectonophysics* **295**, 199
[3] Austrheim H, Boundy T M 1994 *Science* **265**, 82
[4] Fondriest M, Smith S A F, Candela T, Nielsen S B, Mair K, Di Toro G 2013 *Geology* **41**, 1157
[5] Rice J R 2006 *J. Geophys. Res.* **111**, B05311, doi:10.1029/2005JB004006
[6] Cornelio C, Spagnuolo E, Di Toro G, Nielsen S, Violay M 2019 *Nature Comm.* **10**, 1274
[7] Burridge R, Knopoff L 1967 *Bull. Seism. Soc. Am.* **57**, 341
[8] Bridgman P W 1936 *J. Geol.* **44**, 653
[9] Spray J G 1987 *J. Struct. Geol.* **9**, 49
[10] Tullis T E, Weeks J D 1986 *Pure Appl. Geophys.* **124**, 383
[11] Shimamoto T, Tsutsumi A 1994 *J. Tect. Res. Group Japan* **39**, 65
[12] Reches Z, Lockner D A 2010 *Nature* **467**, 452
[13] Di Toro G *et al* 2010 *Rendiconti Lincei* **21**, 95
[14] Tsutsumi A, Shimamoto T 1997 *Geophys. Res. Lett.* **24**, 699
[15] Aretusini S, Meneghini F, Spagnuolo E, Harbord C, Di Toro G 2021 *Nature Comm.* **12**, 2481
[16] Di Toro G, Goldsby D L, Tullis T E 2004 *Nature* **427**, 436
[17] Green H W, Shi F, Bozhilov K, Xia G, Reches Z 2015 *Nature Geoscience* **8**, 448
[18] De Paola N, Holdsworth R E, Viti C, Collettini C, Bullock R 2015 *Earth Planet. Sci. Lett.* **431**, 48
[19] Pozzi G, De Paola N, Nielsen S B, Holdsworth R E, Tesei T, Thieme M, Demouchy S 2021 *Nature Geoscience* **14**, 1
[20] Di Toro G *et al* 2011 *Nature* **471**, 494
[21] Murphy S, Di Toro G, Romano F, Scala A, Lorito S, Spagnuolo E, Aretusini S, Festa G, Piatanesi A, Nielsen S 2018 *Earth Planet. Sci. Lett.* **486**, 155
[22] Aretusini S, Núñez-Cascajero A, Spagnuolo E, Tapetado A, Vázquez C, Di Toro G 2021 *Geophys. Res. Lett.*, **48**, e2020GL091856
[23] Viesca R C, Garagash D I 2015 *Nature Geoscience* **8**, 875
[24] Renard F, McBeck J, Kandula N, Cordonnier B, Meakin P, Ben-Zion Y 2019 *Proc. Nat. Acad. Sci.* **116**, 16234